Wind and Structures, *Vol. 30, No. 3 (2020) 219-229*
DOI: https://doi.org/10.12989/was.2020.30.3.219

Correlation of internal and external pressures and net pressure factors for cladding design

Geeth G. Bodhinayake*, John D. Ginger[a] and David J. Henderson[b]

Department of Civil Engineering, James Cook University, James Cook Drive, Townsville, QLD 4811, Australia

(Received June 25, 2018, Revised December 9, 2019, Accepted December 22, 2020)

Abstract. Net pressures on roofs and walls of buildings are dependent on the internal and external pressure fluctuations. The variation of internal and external pressures are influenced by the size and location of the openings. The correlation of external and internal pressure influences the net pressures acting on cladding on different parts of the roof and walls. The peak internal and peak external pressures do not occur simultaneously, therefore, a reduction can be applied to the peak internal and external pressures to obtain a peak net pressure for cladding design. A 1:200 scale wind tunnel model study was conducted to determine the correlations of external and internal pressures and effective reduction to net pressures (i.e., net pressure factors, F_C) for roof and wall cladding. The results show that external and internal pressures on the windward roof and wall edges are well correlated. The largest $C_{\check{p},net}$, highest correlation coefficient and the highest F_C are obtained for different wind directions within 90° $\leq \theta \leq$ 135°, where the large openings are on the windward wall. The study also gives net pressure factors F_C for areas on the roof and wall cladding for nominally sealed buildings and the buildings with a large windward wall opening. These factors indicate that a 5% to 10% reduction to the action combination factor, K_C specified in AS/NZS 1170.2(2011) is possible for some critical design scenarios.

Keywords: external pressure; internal pressure; net pressure; correlation; combination factor; pressure factor; wind load; standard

1. Introduction

The wind-induced pressure inside a building depends on the external pressure, size and location of openings in the envelope, building porosity, and building volume. The surrounding external pressures on the envelope produce small internal pressures attributed to porous holes or construction gaps in a nominally sealed building. Strong winds or windborne debris can damage the envelope of a building and create a large opening, which produces large internal pressure fluctuations. An opening on the windward wall generates a positive internal pressure, and in combination with negative external pressure can produce large net pressures on cladding and structural elements on the roof and walls.

Full-scale and model-scale tests have been conducted to study the wind-induced internal pressure in buildings with various opening configurations. The phenomenon of Helmholtz resonance, volume scaling for internal pressure and governing equations have been established through model scale and theoretical studies by Liu (1975 and 1981), Holmes (1979), and Vickery (1986). These outcomes have been used as the foundation for analysing internal pressures in nominally sealed buildings and building with large openings conducted by Oh *et al*. (2007), Sharma *et al*. (2003), Ginger *et al*. (2010), Guha *et al*. (2011 and 2013), Kim *et al*. (2013) and Xu *et al*. (2014 and 2017). These studies have shown that internal pressure fluctuations depend on the size and location of openings in the envelope, the volume of the building, and the external pressure fluctuations at the openings. Vickery (1986) found that the internal pressure fluctuations in a building with a dominant opening is significantly reduced when the background leakage area is greater than 10% of the dominant opening size.

Ginger *et al*. (1997) conducted a full-scale experiment on the WERFL test building at Texas Tech and validated the results of model scale and theoretical studies. They showed that internal pressure energy increases close to the Helmholtz frequency in a building with a single dominant opening. Humphreys *et al*. (2019) carried out a controlled, full-scale experimental study with a range of single windward openings to determine the threshold size of the opening required for the peak internal pressure to reach the peak external pressure at the opening.

Model-scale studies by Beste *et al*. (1997) and Sharma *et al*. (2005), and full-scale studies by Ginger and Letchford (1999) have discussed the correlation of external and internal pressures on different parts of the envelope. These studies show that the net pressures across the envelope are related to the correlation of external and internal pressures. The internal and external pressures are well correlated at the upwind roof edge but are poorly correlated at roof corners in a building with a windward wall opening.

*Corresponding author, Ph.D. Student
E-mail: geeth.bodhinayake@my.jcu.edu.au
[a]Professor
E-mail: john.ginger@jcu.edu.au
[b]Ph.D.
E-mail: david.henderson@jcu.edu.au

http://www.techno-press.com/journals/was&subpage=7
ISSN: 1226-6116 (Print), 1598-6225 (Online)

(a) Three-wall shed (gable end wall open)

(b) Large opening in the middle of the gable end wall

Fig. 1 Typical sheds with large openings

Peak external suction pressures combine with peak positive internal pressures to produce the design net (external – internal) negative pressure and vice versa. The peak external and internal pressures do not occur at the same instant; thus, design net pressures derived from applying these peak pressures will be conservative. Action combination factors (K_C) estimated from limited studies are specified in the standard for wind actions AS/NZS 1170.2 (2011) to account for this lack of correlation.

This paper analyses the internal pressure and net pressure in three common industrial type open plan building cases: a nominally sealed building, a 3-wall building with an open gable end wall shown in Fig. 1(a) and a building with a single large opening in the middle of the gable end wall (Fig. 1(b)). The correlation of external and internal pressures on selected roof and wall areas are determined and the combined effect of external and internal pressures on the roof and wall cladding is studied, and net pressures factors (F_C) that account for the lack of correlation of external and internal pressures are derived. These F_C values are compared with combination factors (K_C) listed in AS/NZS 1170.2(2011).

2. Wind tunnel setup

A 80 m long × 40 m wide × 20 m high industrial building was constructed at a length scale $L_r = L_{model\text{-}scale} / L_{full\text{-}scale}$ of 1/200 and tested in the 2.5 m wide × 2 m tall × 22 m long Boundary Layer Wind Tunnel at the Cyclone Testing Station, James Cook University in Townsville, Australia. The approach Atmospheric Boundary Layer was satisfactorily simulated at the length scale of 1/200 for AS/NZS 1170.2 (2011) terrain category 2, as shown by the measured mean velocity and turbulence intensity profiles in Figs. 2(a)-(b). The measured mean wind speed at the roof height ($\overline{U}_h$) is about 11 m/s and turbulence intensity (I_u) at roof height is 0.18. Fig. 2(c) shows the velocity spectrum of the approach wind flow which compares satisfactorily with the Von-Karman spectrum at a length scale of 1/200. The measured longitudinal length scale of turbulence in the wind tunnel at the building roof height (100 mm) is 0.436 m which is equivalent to 87.2 m in full-scale. This wind tunnel study has slightly lower length scale of turbulence compared to the full-scale value of 107 m in WERLF building (Tieleman *et al*. 1997) and 101 m derived from AS/NZS 1170.2 (2011).

Table 1 Building configurations tested

Case #	Description	Opening size	Opening to wall area* Ratio
1	Nominally sealed	60 × 3 mm dia. on all walls	0.003
2	LO6 on Wall #4	190 mm × 95 mm	0.92
3	LO5 on Wall #4	80 mm × 40 mm	0.16

*wall area–the whole surface area of Wall #4 (100×200 mm2)

The model-scale building has an additional 400 mm × 200 mm × 600 mm volume below the turn-table in the wind tunnel to satisfy volume scaling requirements as shown in Fig. 3. Internal pressures are measured at four locations inside the building as shown in Fig. 3. All these internal pressure taps experience the same pressure fluctuations, and the average of four internal pressures is used in the analysis. The external pressures are measured at four locations on the roof (R1, R2, R3, and R4), two locations on Wall #1 (W1 and W2) and seven locations (1 to 7) on Wall #4 as shown in Fig. 4. The pressure taps R1, R2 and W1 are at the windward edge of the roof and sidewall, while R3 and R4 are in the middle of the roof, and W2 is at the middle of the sidewall. Wall #4 becomes the windward wall for wind approaching direction, θ = 90° (Fig. 3 and 4).

Pressure taps were connected to pressure transducers in the calibrated Turbulent Flow Instrument (TFI) system using 1200 mm long × 1.2 mm diameter flexible tubes. The percentage error in pressure measurements is about 2% in the calibrated TFI system when corrected for the distortions caused by connecting flexible tubes. Further, the TFI system also accommodates simultaneous pressure measurements.

Table 1 describes the three-building configurations tested: Case #1, a leaky, nominally sealed building with 60 × 3 mm holes uniformly distributed on the walls. Case #2, whole gable wall open with opening LO6, and Case #3 building with opening LO5 equal to 16% of Wall #4.

External and internal pressure time history data were measured for 16 seconds at a frequency of 625 Hz. The internal volume of the model was distorted to satisfy scaling requirements as explained by Holmes (1979) with an additional volume under the turntable of the wind tunnel (Fig. 3). Correspondingly, the volume ratio V_r between

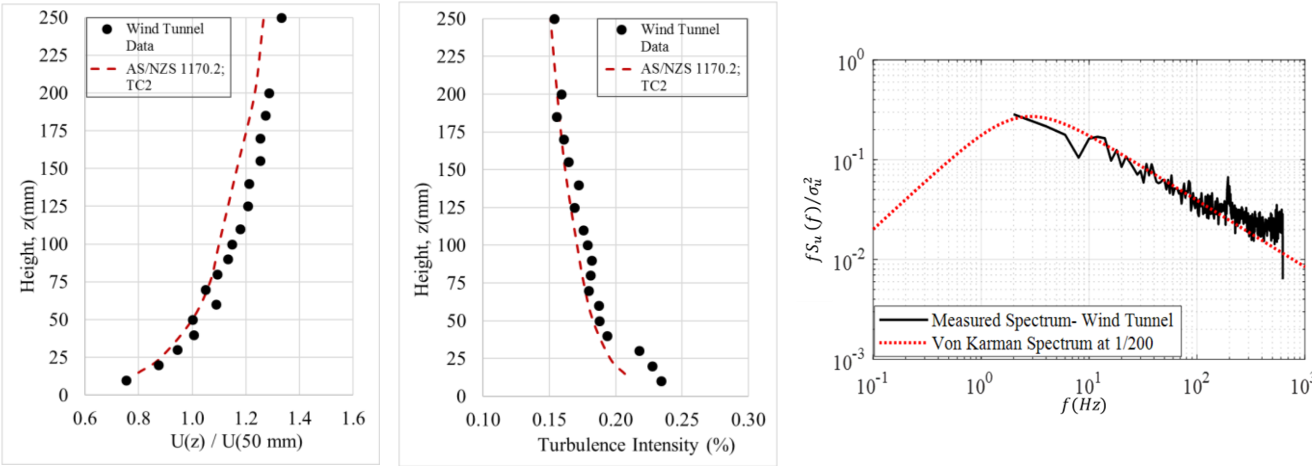

(a) Wind speed profile (b) Wind direction profile (c) Velocity Spectrum at roof height (100 mm)

Fig. 2 Boundary layer wind profile simulated in the wind tunnel at a length scale of 1/200

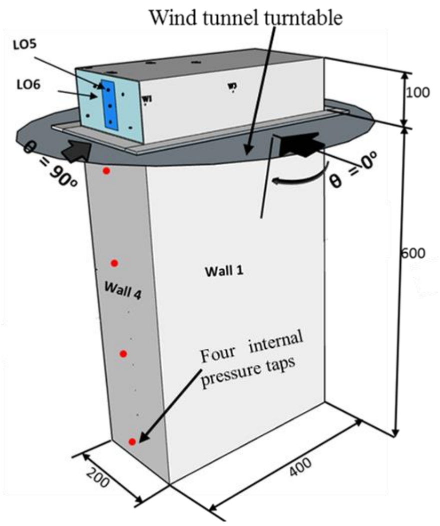

Fig. 3 Wind tunnel model - 1:200 scale (all dimensions are in millimetres)

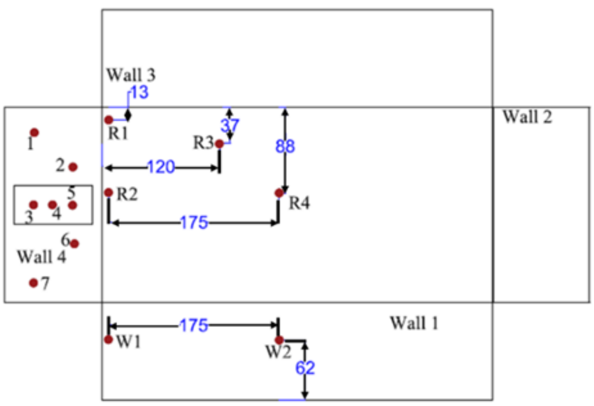

Fig. 4 Tap layout - External pressure (all dimensions are in millimetres)

model scale and full scale is maintained as$[V]_r = [L]_r^3/[U]_r^2$, where the length-scale ratio $[L]_r$=1/200 and the velocity scale ratio $[U]_r \approx 0.4$. The approach flow velocity ratio is defined as $[U]_r = [L]_r/[T]_r$, where $[T]_r$ is time scale ratio for model to full-scale, which is denoted as $[T]_r = \frac{1}{200 \times 0.4} = 0.0125$. The equivalent full-scale time, (T_{fs}) is defined as $T_{fs} = \frac{T_{ms}}{0.0125}$, giving model scale time (T_{ms}) 16 s equivalent to about 20 min in full scale.

The time (t) varying external pressure, $p_e(t)$ and internal pressure, $p_i(t)$ were recorded and pressure time histories were converted into pressure coefficients ($C_p(t) = p(t)/(0.5\rho_a \bar{U}_h^2)$). The mean, standard deviation, maximum and minimum, external pressure coefficients and internal pressure coefficients, are also obtained for each approach wind direction as follows

$$C_{\bar{p}} = \frac{\bar{p}}{(1/2)\ \rho_a \bar{U}_h^2}, \qquad C_{\sigma p} = \frac{\sigma_p}{(1/2)\ \rho_a \bar{U}_h^2},$$

$$C_{\hat{p}} = \frac{\hat{p}}{(1/2)\ \rho_a \bar{U}_h^2}, \qquad C_{\check{p}} = \frac{\check{p}}{(1/2)\ \rho_a \bar{U}_h^2}$$

where, $\bar{p}$, σ_p, $\hat{p}$ and $\check{p}$ are the mean, standard deviation, maximum, and minimum pressures in each 16 s period, $\bar{U}_h$ is the mean wind speed at the roof-height (h = 100 mm), and ρ_a is the density of air.

The net pressure coefficient, $C_{p,net}(t) = C_{pe}(t) - C_{pi}(t)$ is generated for each pressure tap location and for each approach wind direction. The external and internal pressures acting towards the surface is defined as positive and the suction pressures acting away from the surface is negative. Further, the net pressure acting inwards is defined as positive.

The external and internal pressures were measured simultaneously for each run and the pressure time history data were recorded for five repeat runs for each approaching wind direction from θ = 90° to 270° in 5° intervals. The mean, maximum, minimum and standard deviation of external, internal and net pressure coefficients are obtained for each individual run, an average of the five runs are presented in this paper.

3. Theory

3.1 Building with a single opening

The conservation of mass specifies that the mean inflow equals the mean outflow and was used by Liu (1975) to derive Eq. (1). Here, A_W is the total windward opening area (though which air flows into the building), A_L is the total leeward opening area (though which air flows out of the building), $C_{\bar{p}_i}$ is the mean internal pressure coefficient, $C_{\bar{p}W}$ and $C_{\bar{p}_L}$ are the mean external pressure coefficients at windward and leeward openings, respectively.

$$C_{\bar{p}_i} = \frac{C_{\bar{p}W}}{1 + (A_L/A_W)^2} + \frac{C_{\bar{p}_L}}{1 + (A_W/A_L)^2} \quad (1)$$

Determination of $C_{\bar{p}i}$ in a building from Eq. (1) for a given A_w/A_L ratio is similar to the quasi-steady pressure coefficients given in wind loading standards (i.e. AS/NZS 1170.2, 2011). In a building with a single windward opening ($A_L = 0$), Eq. (1) shows that the mean internal pressure follows the mean external pressure at the windward opening. Humphreys *et al.* (2019) measured internal and external pressures in a sealed Full-Scale Test Enclosure with a range of "single" openings on the windward wall in atmospheric wind flows and found that the ratio of mean internal to external pressure is approximately 1.0, in agreement with Eq. (1). Therefore, LO5 and LO6 openings in the study are considered as single large openings (i.e. dominant) in the envelope.

Holmes (1979) studied internal pressure fluctuations in a building with a large opening using the Helmholtz resonator model, and described the internal pressure dynamics using the second order differential equation given by Eq. (2). It describes the motion of an air slug through a single opening into and out of a building in terms of first ($\dot{C}_{pi}(t)$) and second ($\ddot{C}_{pi}(t)$) derivatives of $C_{pi}(t)$ with respect to time, t. The first term of Eq. (2) represents the inertia of the flow, while the second term represents the damping of the system in terms of, a_s- the speed of sound, A-area of the large opening, V- effective volume of the building, C_I-Inertial coefficient, C_L - Loss coefficient. Internal pressure resonance occurs at the Helmholtz frequency, $f_H = 1/2\pi\sqrt{a_s^2\sqrt{A}/(C_I V)}$.

$$\frac{C_I V}{a_s^2\sqrt{A}}\ddot{C}_{pi}(t) + C_L\left(\frac{V\bar{U}_h}{2a_s^2 A}\right)^2 \dot{C}_{pi}(t)\left|\dot{C}_{pi}(t)\right| + C_{pi}(t) = C_{pe}(t) \quad (2)$$

3.2 Correlation of external and internal pressure

The cross-correlation coefficient between the external and internal pressures ($r_{p_e p_i}$) given in Eq. (3) is defined as a function of lag time (τ) of internal pressure relative to the external pressure over the time period observed (T). Cross correlations were obtained for the 16 s time histories of internal and external pressures at each tap location on the building, and are presented for a lag time τ = 0, as $r_{p_e p_i}(0)$ for each wind direction.

$$r_{p_e p_i}(\tau) = \frac{1}{T \times C_{\sigma p_e} \times C_{\sigma p_i}}\int_0^T \left[\left(C_{pe}(\mathrm{t}) - \mathrm{C}_{\bar{p}\mathrm{e}}\right) \times \left(C_{pi}(\mathrm{t}+\tau) - \mathrm{C}_{\bar{p}i}\right)\right]dt \quad (3)$$

Positive internal pressures and negative external pressures are negatively correlated at zero lag time, and the negative internal pressure and negative external pressure are positively correlated. Sharma *et al.* (2005) studied the correlation coefficients of area-averaged external pressures and internal pressure on the roof corner and windward edge for two wall opening cases. They recorded correlation coefficients up to -0.64 on windward roof corners of the building with a central windward opening and up to -0.4 on roof corners of the building with an opening at the opposite end of the windward wall to the roof corner analysed.

3.3 Net pressure factors

Fluctuating pressures on the external and internal surfaces of a building are not well correlated (Beste *et al.* 1997, Sharma *et al.* 2005), and the magnitude of peak net pressures are less than the difference between peak external and peak internal pressure, ($C_{\check{p},net} < \left(C_{\check{p}e} - C_{\hat{p}i}\right)$ and $C_{\hat{p},net} < \left(C_{\hat{p}e} - C_{\check{p}i}\right)$). A net pressure factor (F_C) defined by Eq. (4) provides a measure of this lack of correlation of external and internal pressures. Peak net, external and internal pressures for each approach wind direction, θ are used to derive the net pressure factors. The net pressure factors are only derived for critical outward acting net pressures (negative), and higher F_C values represent a smaller reduction to the difference in peak pressures.

$$F_C(\theta) = \frac{C_{\check{p},net}(\theta)}{C_{\check{p}e}(\theta) - C_{\hat{p}i}(\theta)} \quad (4)$$

The wind loading standard AS/NZS 1170.2 (2011) specifies combination factors, K_c similar to the net pressure factor, to account for the lack of correlation of pressures on different surfaces that combine for a single reaction force. Here, K_c is applied to the peak external and internal pressures derived from a 90° quadrant of wind directions. That is, for pressures on two contributing surfaces (i.e. large external and internal pressure), AS/NZS 1170.2 (2011) gives a K_c of 0.9, where $C_{\check{p},net} = 0.9\left(C_{\check{p}e} - C_{\hat{p}i}\right)$.

4. Results and discussion

External pressures measured on Wall #4 of the nominally sealed building model are used to obtain the area-averaged external pressures on areas of LO5 and LO6. Area-averaged external pressures on LO6 were derived by averaging the external pressures on the seven taps (1 to 7) on Wall #4, and area-averaged external pressures on LO5 were derived by averaging the external pressure on three taps (3 to 5) on the LO5.

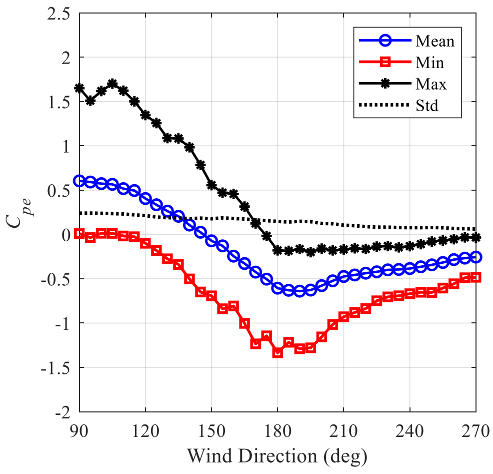

(a) LO6 (Case #1)

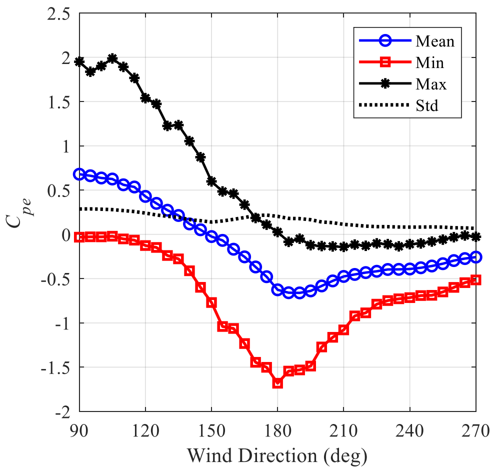

(b) LO5 (Case #1)

Fig. 5 Area-averaged mean, minimum, maximum and standard deviation C_{pe} on the areas of LO5 and LO6 from the nominally sealed configuration, for $\theta = 90^{o} - 270^{o}$

Figs. 5(a) and 5(b) show these area-averaged external pressures applied to LO6 (Case #2) and LO5 (Case #3) for wind directions 90° to 270° from the nominally sealed configuration (Case #1). The area-averaged mean external pressure coefficients on LO6 and LO5 are about +0.6 when these areas are on the windward wall (θ = 90°). The largest $C_{\hat{p}e}$ and $C_{\check{p}e}$ for LO6 (whole wall opening) of +1.7 and -1.34 occurred at θ = 105° and 180°, when the LO6 is on the windward and sidewall, respectively. Additionally, $C_{\hat{p}e}$ on LO5 is 18% higher than LO6 for wind directions $90° \leq \theta \leq 120°$, and $C_{\check{p}e}$ is 25% more negative for wind directions 165° to 195°. The increasing lack of spatial correlation with increasing area results in a reduction in the positive and negative peak pressures with increasing area (as LO6 is 6 × LO5).

Mean, standard deviation, minimum and maximum internal pressure coefficients for Cases #1, #2 and #3 are presented in Figs. 6(a) - 6(c) respectively. Fig. 6(a) shows approximately constant $C_{\bar{p}i}$, $C_{\hat{p}i}$ and $C_{\check{p}i}$ of -0.16, -0.02 and -0.3 respectively and a $C_{\sigma pi}$ of nearly zero for all wind directions. The mean internal pressure is small in comparison to the area-averaged external pressures on Wall #4 (Fig. 5(a)). The restricted flow in and out through the porous holes around the building envelope damped the internal pressure fluctuations in the building.

Figs. 6(b) and(c) show that mean internal pressures are positive and large when the approaching wind blows towards the openings (i.e. θ = 90° – 135°). The highest $C_{\bar{p}i}$ is about +0.5 and +0.6 for Case #2 and #3 respectively when the opening is on the windward wall (θ = 90°). Further, the highest mean suction internal pressure coefficient is about -0.7 for Case #2 at θ = 180° and for Case #3 at θ = 190° when the opening is on the sidewall. Additionally, $C_{\hat{p}i}$ of +1.92 and +2.26 for Case #2 and #3 respectively are 12% and 13% greater than the area-averaged $C_{\hat{p}e}$ on the opening areas of LO6 and LO5 at θ = 90°, and $C_{\check{p}i}$ of -1.25 and -1.35 for Case #2 and #3 respectively are 8% greater and 3% less than the area-averaged $C_{\check{p}e}$ applied on the opening areas of LO6 and LO5 at θ = 190°. These results show that peak internal pressures in Case #3 are higher than Case #2 for wind angles 90° to 270°.

The size of the opening is the main difference between Case #2 and Case #3 which increases the mass flow rate into and out from the building in Case #2 compared to Case #3 and develops different internal pressures in the building. Further, as shown in Figs 5(a) - 5(b) and 6(b) - 6(c), when the building contains a single large wall opening, $C_{\bar{p}i}$ approximately equals to $C_{\bar{p}e}$ in Case #2 and #3 which satisfies the Eq. (1), which also in agreement with the full-scale study by Humphreys *et al.* (2019).

Fig. 7 shows the area-averaged external pressure spectrum on Wall #4 and internal pressure spectra for Cases #1, #2 and #3 for θ = 90°. The internal pressure fluctuations for Case #1 (nominally sealed building), where energy sharply decreases at about 2 Hz are significantly less than Cases #2 and #3. The internal pressure spectra for Cases #2 and #3 follow the external pressure spectrum of Wall #4 until about 4 Hz, where the energy in the internal pressure fluctuations exceed the external pressure fluctuations as they approach their respective Helmholtz resonance frequencies, f_H. The internal pressure spectra decrease rapidly compared to the area-averaged external pressures on the wall, beyond these frequencies.

Helmholtz resonance is observed at f_H of 38 Hz in the 3-wall building (Case #2) which has an opening area to wall area ratio about 0.92. Additionally, Helmholtz resonance occurred at lower f_H of 32 Hz for Case #3 which is consistent with the Helmholtz frequency equation in Section 3.1 and the energy content in the internal pressure spectrum is greater in Case #3 than Case #2 at the orthogonal wind direction to the opening. The inertial coefficient, C_I is calculated as 4.31 for Case #2 and 2.56 for Case #3 using the measured Helmholtz frequencies f_H, where a_s = 340m/s, A (Case #2) = 0.018m^2, A (Case #3) = 0.0032m^2,
V = 0.056m^3. Vickery (1992), Xu *et al.* (2014) and Humphreys *et al.* (2019) stated that a range of C_I values have been derived typically in the range of 0.8 to 2.0 from wind tunnel and full-scale studies, however, no other

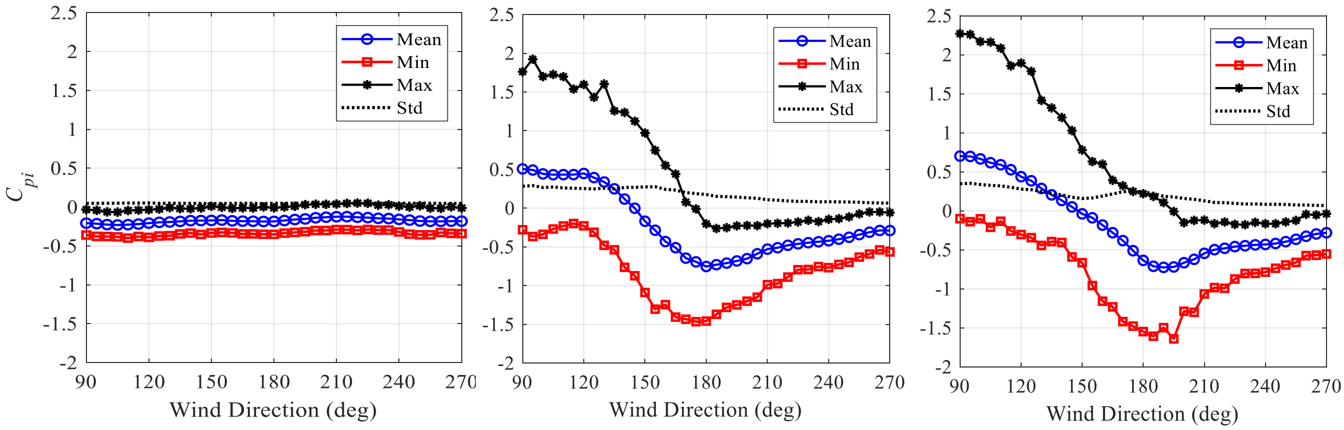

(a) Case 1 (b) Case 2 (c) Case 3

Fig. 6 Mean, standard deviation, minimum and maximum internal pressure coefficients for $\theta = 90^o - 270^o$

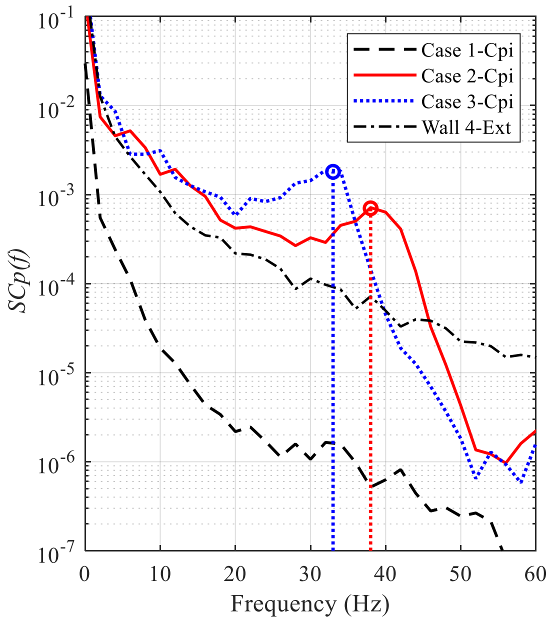

Fig. 7 Area-averaged windward wall external and internal pressure spectra at $\theta = 90^o$

studies have examined such a large opening (i.e., 3-wall building) before.

Figs. 8(a)-8(f) show the negative net pressure coefficient, $C_{\breve{p},net}$ on roof taps (R1 to R4) and wall taps (W1 and W2) for Cases #1, #2 and #3 for the wind directions, θ = 90° to 270°. The largest minimum net pressure is experienced at the windward corner (R1) for all Cases #1, #2 and #3 within the wind direction range 90° ≤ θ ≤ 135°, due to flow separation at the leading edge of the roof for the cornering winds and also due to high positive internal pressures in Cases #2 and #3. $C_{\breve{p},net}$ of -5.34 (θ = 130°) for Case #1, -7.79 (θ = 130°) for Case #2 and -7.39 (θ = 105°) for Case #3 were recorded on roof corner (R1), as shown in Figs. 8(a)-(c). These $C_{\breve{p},net}$ on the roof corner of the building with a large windward opening is consistent with the study by Ginger and Letchford (1999) for a full-scale building with a 0.8m^2 opening on the windward wall. Figs. 8(a)-8(c) further show that $C_{\breve{p},net}$ on the roof pressure taps from Case #1, #2 and #3 have similar variations for 150° ≤ θ ≤180° (i.e., R1, R2 and R3 decrease from -3.0. to -0.5 and R4 decreases from -2.0 to -0.5) suggesting the different large opening sizes do not significantly affect $C_{\breve{p},net}$.

The largest $C_{\breve{p},net}$ is experienced at the windward edge of the Wall #1 (W1) in all Cases #1, #2 and #3 within the wind direction range 90° ≤ θ ≤ 135°. The flow separation at the edge of the opening LO6 creates higher suction pressures in Case #2 at θ = 90° which generates the larger $C_{\breve{p},net}$ of -4.7 for W1, although the positive internal pressure in Case #2 is less than Case #3 (see Figs. 6(b) and (c)). Further, Figs. 8(d)-8(f) show that $C_{\breve{p},net}$ decreases along the sidewall (W1 to W2) from the leading edge of the building for θ = 90° to 135° and external suction pressures on W1 and W2 are almost equal for θ = 160° to 200°.

4.1 Correlation of external and internal pressures

Figs. 9(a)-9(c) show the correlation coefficient, $r_{p_e p_i}(0)$ on the roof cladding for Cases #1, #2 and #3 for the wind directions θ = 90° to 270°. The internal pressure fluctuations are negative in Case #1 (see Fig. 6(a)), and the internal and external pressures are positively correlated, where $r_{p_e p_i}(0)$ is less than 0.5 for all roof taps for all wind directions, as shown in Fig. 9(a), for Case #1.

Figs. 9(b)-9(c) show that external roof suction pressures at the roof windward edge (R1 and R2) are well correlated negatively with the positive internal pressures for 90°≤ θ ≤ 135°, while external suction and negative internal pressures are positively correlated, for 180°≤ θ ≤270°.

The external pressures on R3 and R4 on the middle of the roof are poorly correlated with the internal pressure, which explains the lower net pressure at R3 and R4 compared to R1 and R2. These results show that, $r_{p_e p_i}(0)$ decreases towards the middle of the roof for θ= 90° to 135°. $r_{p_e p_i}(0)$ obtained for Case #3 is in agreement with the results obtained by Xu and Lou (2017). The outcomes also matched the full-scale results obtained by Ginger and Letchford (1999) who found that the large external suction pressures at the windward roof edge were well-correlated

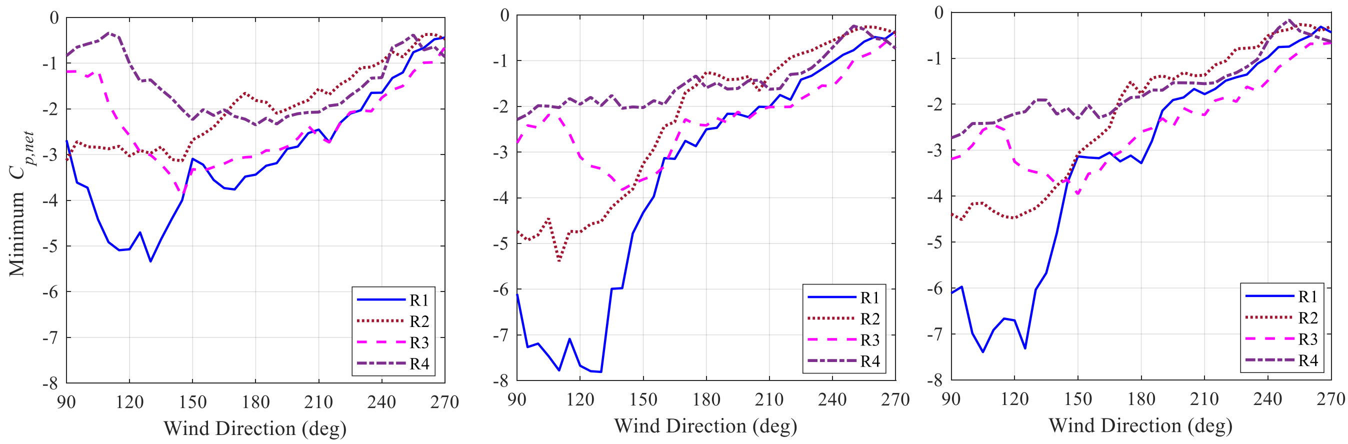

(a) Case 1 (b) Case 2 - LO6 (c) Case 3 – LO5

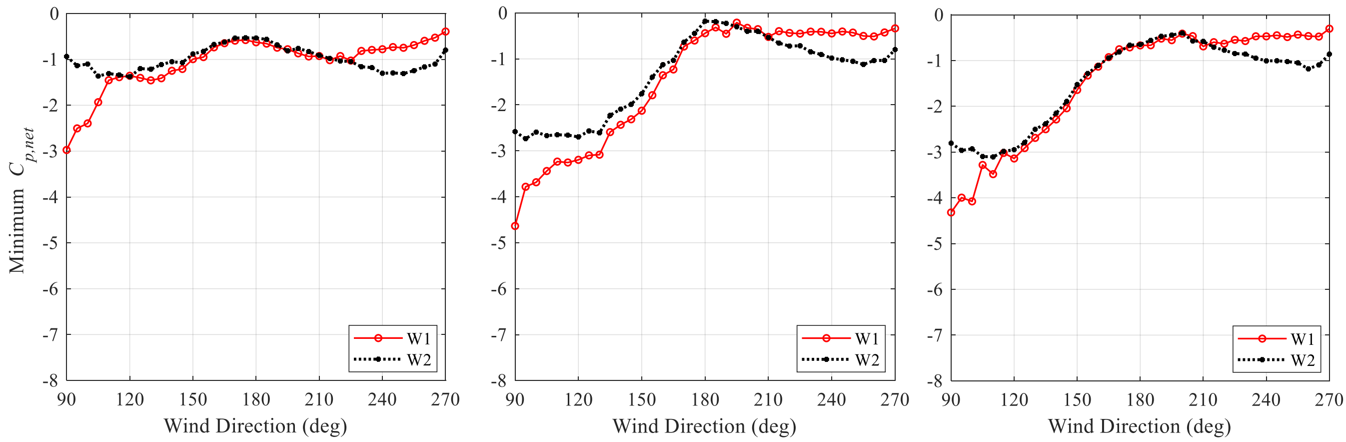

(d) Case 1 (e) Case 2 - LO6 (f) Case 3 – LO5

Fig. 8 Peak net pressure, $C_{\breve{p},net}$ on the roof and Wall # 1, $\theta = 90^{o} - 270^{o}$

with large positive internal pressures leading to large net pressures on the region that is most vulnerable to cladding failure.

For wind directions 90°≤ θ ≤135°, $r_{p_e p_i}(0)$ varied between -0.4 to -0.7 at the windward roof edge (R1 and R2) for Cases #2 and #3, which is similar to results obtained by Sharma *et al*. (2005) from model scale tests of a building with a 40 mm × 20 mm opening. The correlation of external and internal pressures in the middle of the roof (R3 and R4) for Cases #2 and #3 are similar to the results presented for three different single dominant opening cases by Xu and Lou (2017) for openings on the windward wall and sidewall.

For the nominally sealed building (Case #1), Fig. 9(d) shows the correlation of external and internal pressures of W1 and W2 on Wall #1 for θ = 90° to 270°. The fluctuating external pressures around the nominally sealed building cause the small negative internal pressure fluctuations. Fig. 9(a) shows that external suction and negative internal pressures are positively correlated at W1 and W2 for Case #1. The moderately correlated external and internal pressures produced low minimum net pressures at the wall cladding of the nominally sealed building.

The Figs. 9(e)-9(f) show that the $r_{p_e p_i}(0)$s on the sidewalls of Cases #2 and #3 are negative for 90°≤ θ ≤135° and smaller than the correlation coefficient of roof windward edge. Further, compared to the external pressure at the middle of the sidewall (W2), external pressures close to the leading edge (W1) and internal pressures are moderately correlated. The $r_{p_e p_i}(0)$ is slightly higher at W1 for the whole wall opening (Case #2) since the pressure tap is closer to the opening compared to the opening at the middle of the gable wall (Case #3). For wind directions 225°≤ θ ≤270°, the opening for Cases #2 and #3 are on the leeward wall generating negative internal pressures that are positively correlated with external suction pressures on the middle and end of Wall #1, W2 and W1 respectively. Further, size of the opening does not significantly affect the correlation of external and internal pressures of the wall cladding as shown in Fig 9(e)-9(f) and $r_{p_e p_i}(0)$ decreases along the sidewall from the windward edge similar to that described by Xu and Lou (2017).

4.2 Net pressure factors on roof and wall cladding

The net pressure factors (F_C) with approaching wind direction θ are calculated using the minimum net, minimum external and maximum internal pressures, as described by Eq. (4). Increasing correlation between internal and external pressures tend to produce higher $F_C s$ and vice versa.

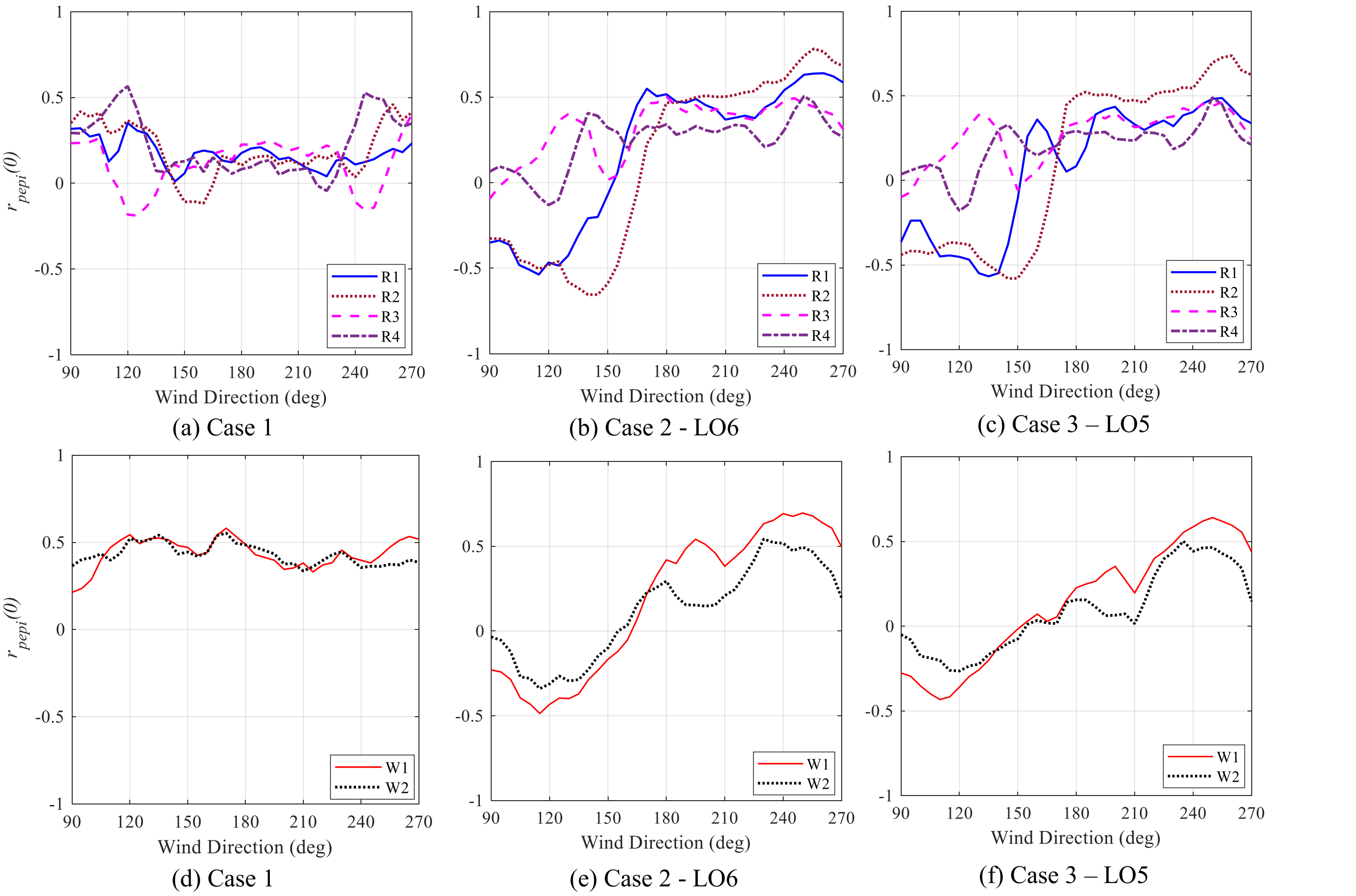

Fig. 9 $r_{p_e p_i}(0)$ on the Roof and Wall #1 for $\theta = 90^o - 270^o$

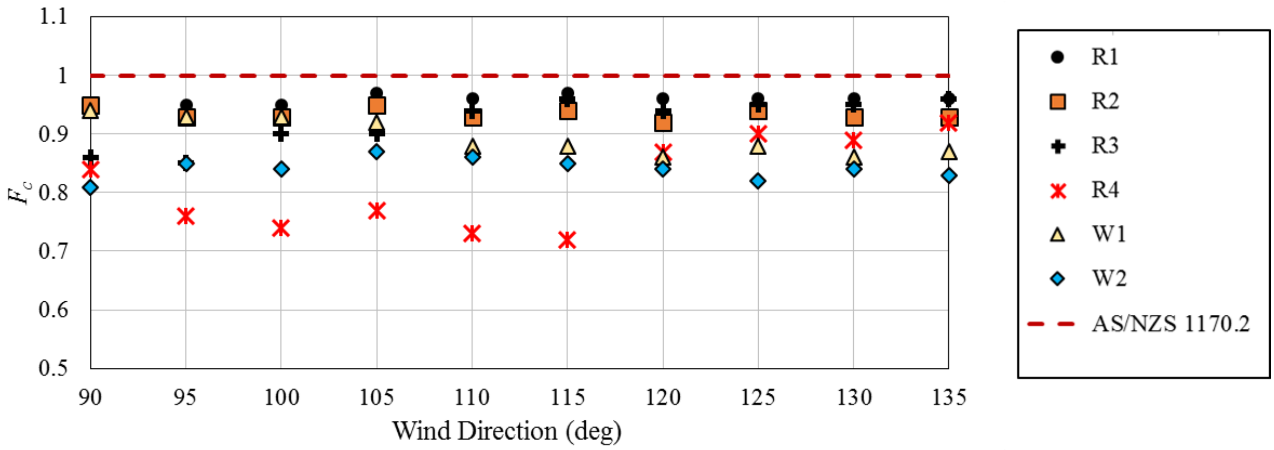

Fig. 10 Net pressure factors, F_C on Roof and Wall #1 for Case # 1: wind directions 90° to 135°

These net pressure factors are compared with the combination factor (K_c), given in AS/NZS 1170.2 (2011). AS/NZS 1170.2 specifies that $K_c = 1$ for net cladding loads when $|C_{pi}| < 0.2$, which accounts for the minor contribution of the internal pressure (i.e. Case #1). For other instances, $K_c = 0.9$ for deriving net cladding loads, when pressures act on two effective surfaces, (i.e., Cases #2 and #3).

Net pressure factors derived for roof and wall taps for Case #1 are presented in Fig. 10 for θ of 90° to 135°. Higher net pressure factors and largest $C_{\breve{p},net}$ do not always occur for the same wind direction; for example, the roof tap R1 experiences the largest $C_{\breve{p},net}$ at $\theta = 135°$, whilst the largest F_C is at $\theta = 105°$. Internal pressures in

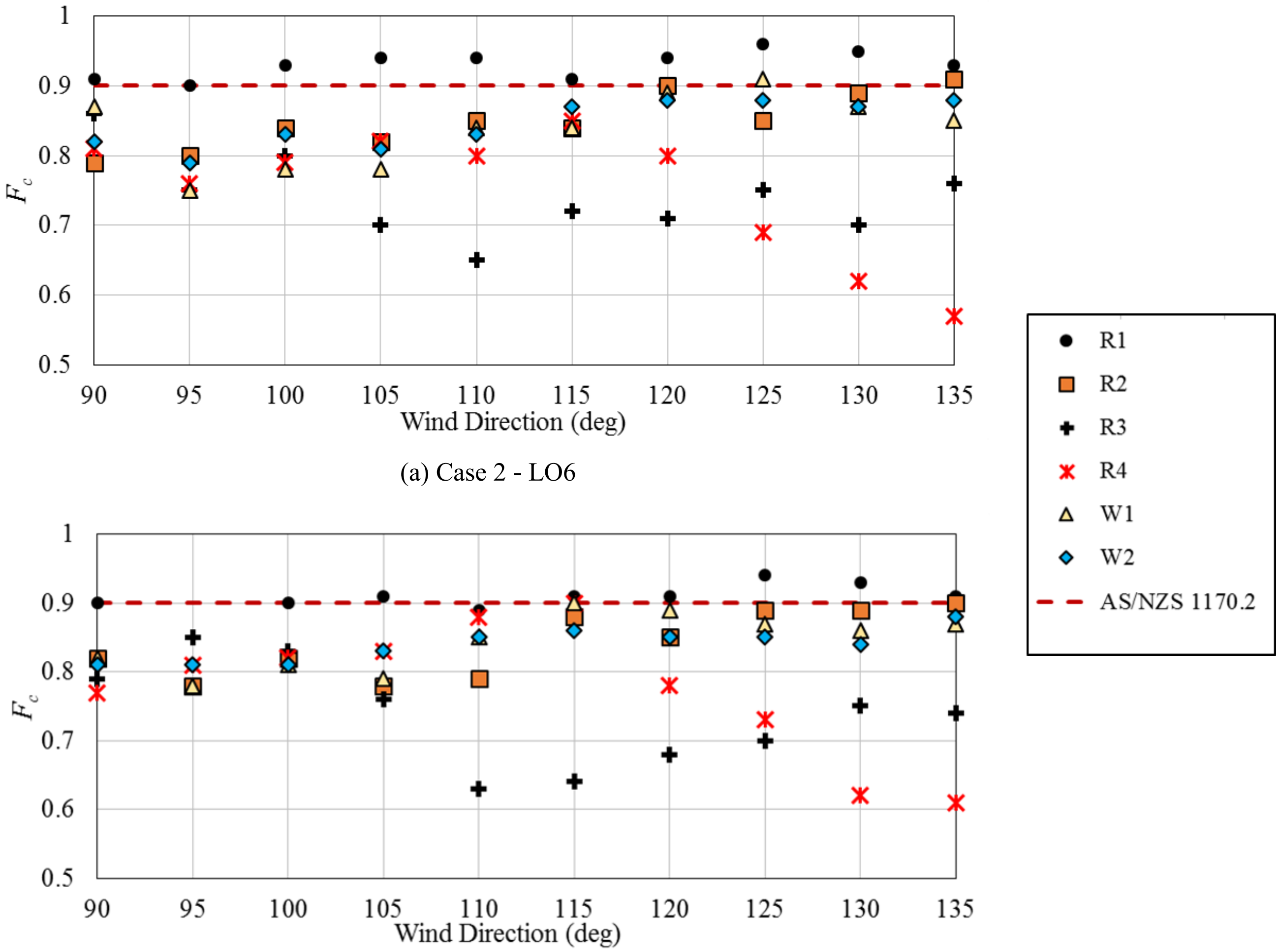

(b) Case 3 – LO5

Fig. 11 Net pressure factors, F_C wind angle range 90º to 135º, Case #2 and Case #3

Case #1 are significantly lower than the negative external pressures, and only have a minor influence on the net pressure factors, thus producing high F_C values on the roof and wall. However, small net pressure factors are derived as shown in Fig. 10, due to the low correlation of external and internal pressures on the roof and wall for Case #1 (see Fig. 9(a) and 9(d)). Fig. 10 further shows that the net pressure factors on windward roof edges (R1 and R2) are about 3% to 5% less than the K_c from AS/NZS 1170.2 (2011), and 10% less for other locations on the roof and wall, of the nominally sealed building.

Figs. 11(a)-11(b) show the net pressure factors, F_C for Cases #2 and #3 for wind directions θ of 90º to 135º. The F_Cs depend on wind direction, location of the tap, and size of the opening and varies between 0.55 to 0.9 for both Cases #2 and #3 as shown in Figs. 11(a)-11(b). The net pressure factors for the roof corner tap (R1) range between 0.9 to 0.96 for Case #2, and 0.8 to 0.94 for Case #3. The largest F_C for roof corners of both Case #2 and #3 were obtained at θ = 125º, which produces the highest net pressures as shown in Figs. 8(b)-8(c). Therefore, F_C can be computed with the wind direction of the largest peak net pressures of the particular cladding location, thus net reduction factor for R2 of 0.84 (θ = 110º) for Case #2 and 0.78 (θ = 95º) for Case #3. Similarly, F_Cs for R3 and R4 at 135º and 90º are about 0.75 and 0.8 and F_Cs for W1 and W2 at 90º are range between 0.8 and 0.85 for Case #2 and #3 respectively, regardless of the opening size. Accordingly, when net reduction factors are compared with $K_c(= 0.9)$ in the AS/NZS 1170.2 (2011), derived F_Cs are 5% higher on roof corner (R1), 5% lower on leading roof and wall edges (R2, W1) and 10% lower on the middle of the roof and wall (R3, R4, W2).

Xu and Lou (2017) derived combination factors for peak external pressures and peak internal pressures for a building with a single dominant opening. Accordingly, the combination factor of 0.43 on roof claddings and 0.96 on wall cladding for peak external pressures and 0.98 for peak internal pressure were introduced to reduce the peak net pressures on the roof and wall due to the lack of correlation of peak external and internal pressures. The net pressure factors, F_C shown in Figs. 10 and 11 closely agree with the results by Xu and Lou (2017).

As shown in Figs. 8, 9 and 11 the largest $C_{\breve{p},net}$,$r_{p_e p_i}(0)$ and F_C for each Case occurs for different approaching wind directions. For example, the highest $C_{\breve{p},net}$, $r_{p_e p_i}(0)$ and F_C were observed for θ =130°, 115° and 125° respectively for the roof corner tap (R1) from Case #2. Hence picking the highest F_C value as the net pressure factor for wind direction range 90°≤ θ ≤135° for Cases #2 and #3 will not represent the actual reduction to net pressures on the roof and wall cladding. The highest peak net, external, and internal pressures within 90°≤ θ ≤135° must be considered when deriving the appropriate F_C for the wind directions 90° to 135°. For example, the highest $C_{\breve{p}net}$ of -7.81 (θ = 130°), highest $C_{\breve{p}e}$ of -6.67 (θ = 130°) and highest $C_{\hat{p}i}$ of 1.92 for R1 of Case #2 within the wind direction 90°≤ θ ≤135° produces F_C of 0.91 which is 5% less than the highest F_C of 0.96 (θ = 125°) shown in Fig. 11(a).

5. Conclusions

The correlation of internal and external pressures, and net pressure factors are obtained using external and internal pressures on a typical industrial type building by carrying out a wind tunnel study at a length scale of 1/200. The net pressure coefficients were obtained at selected point locations on the roof and wall cladding on a nominally sealed building (Case #1) and buildings with a large opening (3-wall building Case #2, and 16% wall opening Case #3). This study shows that;

- The mean and peak internal pressures closely match the area-averaged external pressures at the opening, as indicated by $C_{\bar{p}i} \approx C_{\bar{p}e}$ for Case #2 and #3.
- Large net suction pressures are experienced at windward roof corners (R1) and windward roof edges (R2) due to flow separation at the windward edge for 90°≤ θ ≤135°. The largest $C_{\breve{p},net}$ of -7.79 is recorded at θ = 130° for Case #2, although the largest $C_{\hat{p}i}$ is 1.92 at θ = 90°.
- For the building with the whole gable wall open (Case #2), f_H is about 38 Hz and corresponds to an inertial coefficient,C_I of about 4.31.
- For building with a 16% wall opening at the centre of gable wall (Case #3), f_H is about 32 Hz and corresponds to a C_I of about 2.56.
- The correlations of external and internal pressures $r_{p_e p_i}(0)$ explains the combined effects of internal and external pressures that produce the peak net pressure. $r_{p_e p_i}(0)$s for roof and wall taps on the nominally sealed building is positive and fluctuates between +0.3 and +0.5.
- For the building with a large opening (Cases #2 and #3), external suction pressures and positive internal pressures are negatively correlated at the roof corner, roof windward edge and sidewall for 90°≤ θ ≤135°. The $r_{p_e p_i}(0)$ fluctuates between -0.4 to -0.7 at the roof corner (R1) and at the windward roof edge (R2) which is similar to results obtained by Sharma *et al*. (2005).
- The correlation of external suction pressures and positive internal pressures decrease towards the middle of the roof for Cases #2 and #3 and small $r_{p_e p_i}(0)$ are not significantly influenced by the size of the opening within wind directions 90°≤ θ ≤135°.
- The highest $C_{\breve{p},net}$, $r_{p_e p_i}(0)$ and F_C occur at different wind directions in the critical wind directions 90°≤ θ ≤135°.
- The net pressure factors for the nominally sealed building is about 0.95 on the windward corners and leading edges of roof and sidewall and 0.9 for the rest of roof and sidewall, which suggests a 5% and 10% reduction compared to K_C in AS/NZS1170.2.
- For Cases #2 and #3, F_C on the windward roof corner and leading roof edges are 5% greater than and 5% lower than K_C in AS/NZS 1170.2 respectively.
- The net reduction factor is about 0.8 at the middle of the roof and sidewall of the building with a large gable wall opening, which is a 10% reduction compared to K_C in AS/NZS 1170.

Acknowledgments

The Authors acknowledge the Australian Research Council Linkage Grant, and their partners: the Australian Steel Institute, JDH Consulting and Scott Woolcock Consulting for their support to carry out this research.

References

Beste, F. and Cermak, J.E. (1997), "Correlation of internal and area-averaged external wind pressures on low-rise buildings", *J. Wind Eng. Ind. Aerod.*, **69**, 557-566. https://doi.org/10.1016/s0167-6105(97)00186-4.

Ginger, J.D. (1997), "Internal and net pressures on low-rise full-scale buildings. cyclone structural testing station", Technical Report 45.

Ginger, J.D. and Letchford, C.W. (1999), "Net pressures on a low-rise full-scale building", *J. Wind Eng. Ind. Aerod.*, **83**(1-3), 239-250. https://doi.org/10.1016/s0167-6105(99)00075-6.

Ginger, J.D., Holmes, J.D. and Kim, P.Y. (2010), "Variation of internal pressure with varying sizes of dominant openings and volumes", *J. Struct. Eng.*, **136**(10), 1319-1326. https://doi.org/10.1061/(asce)st.1943-541x.0000225.

Guha, T.K., Sharma, R.N. and Richards, P.J. (2011), "Internal pressure dynamics of a leaky building with a dominant opening", *J. Wind Eng. Ind. Aerod.*, **99**(11), 1151-1161. https://doi.org/10.1016/j.jweia.2011.09.002.

Guha, T.K., Sharma, R.N. and Richards, P.J. (2013), "Internal pressure in a building with a single dominant opening: an experimental and numerical case study", *J. Wind Eng. Ind. Aerod.*, **41**(1), 243-252. https://doi.org/10.3850/978-981-07-8012-8_156.

Holmes, J.D. (1979), "Mean and fluctuating internal pressures induced by wind", Fifth International Conference on Wind Engineering, Fort Collins, Colorado, U.S.A.

Humphreys, M.T., Ginger, J.D. and Henderson, D.J. (2019), "Internal pressures in a full-scale test enclosure with windward wall opening", *J. Wind Eng. Ind. Aerod.*, **189**(2019), 118-124. https://doi.org/10.1016/j.jweia.2019.03.024.

Kim, P.Y. and Ginger, J.D. (2013), "Internal pressures in buildings with a dominant opening and background porosity", *Wind*

Struct., **16**(1), 47-60. https://doi.org/10.12989/was.2013.16.1.047.

Liu, H. (1975), "Wind pressure inside buildings", Proceedings of the 2nd US National Conference on Wind Engineering Research, Colorado State University, Colorado, June.

Liu, H. and Saathoff, P.J. (1981), "Building internal pressure: sudden change", *J. Eng. Mech. Div*., **107**(2), 309-321.

Oh, J.H., Kopp, G.A. and Inculet, D.R, (2007), "The UWO contribution to the NIST aerodynamic database for wind loads on low buildings: Part 3. internal pressures", *J. Wind Eng. Ind. Aerod*., **95**(8), 755-779. https://doi.org/10.1016/j.jweia.2007.01.007.

Sharma, R.N. and Richards, P.J. (2003), "The influence of Helmholtz resonance on internal pressures in a low-rise building", *J. Wind Eng. Ind. Aerod*., **91**(6), 807-828. https://doi.org/10.1016/s0167-6105(03)00005-9.

Sharma, R.N. and Richards, P.J. (2005), "Net pressures on the roof of a low-rise building with wall openings". *J. Wind Eng. Ind. Aerod*., **93**(4), 267-291. https://doi.org/10.1016/j.jweia.2005.01.001.

Standards Australia (2011), "Structural design actions. Part 2 Wind actions", AS/NZS 1170.2:2011.

Tieleman, H.W., Reinhold, T.A. and Hajj, M.R. (1997), "Importance of turbulence for the prediction of surface pressures on low-rise structures", *J. Wind Eng. Ind. Aerod*., **69**, 519-528. https://doi.org/10.1016/s0167-6105(97)00182-7.

Vickery, B.J. (1986), "Gust-factors for internal-pressures in low rise buildings", *J. Wind Eng. Ind. Aerod*., **23**(1-3), 259-271. https://doi.org/10.1016/0167-6105(86)90047-4

Vickery, B.J. and Bloxham, C. (1992), "Internal pressure dynamics with a dominant opening", *J. Wind Eng. Ind. Aerod*., **41**(1-3), 193-204. https://doi.org/10.1016/0167-6105(92)90409-4.

Xu, H., and W. Lou (2017), "Combined effects of internal and external pressures for a building with wall openings", 9th Asia-Pacific Conference on Wind Engineering, Auckland, New Zealand.

Xu, H., Yu, S. and Lou, W. (2014), "The inertial coefficient for fluctuating flow through a dominant opening in a building", *Wind Struct*., **18**(1), 57-67. https://doi.org/10.12989/was.2014.18.1.057.

Xu, H., Yu, S. and Lou, W. (2017), "The loss coefficient for fluctuating flow through a dominant opening in a building", *Wind Struct*., **24**(1), 79-93. https://doi.org/10.12989/was.2017.24.1.079.

FR